# C(sp3)−H bond activation by carboxylate-adduct of osmium tetroxide (OsO4)

# ARTICLE

## C(sp³)–H bond activation by carboxylate-adduct of osmium tetroxide (OsO₄)

Tomohiro Fujimoto,[a] Yuka Hirata,[a] Hideki Sugimoto,*[a] Mayuko Miyanishi,[b] Yoshihito Shiota,[b] Kazunari Yoshizawa*[b] and Shinobu Itoh*[a]

The reaction of osmium tetroxide (OsO₄) and carboxylate anions (acetate: X = AcO⁻ and benzoate: X = BzO⁻) gave 1 : 1 adducts, $[OsO_4(X)]^-$ (**1ˣ**), the structures of which were determined by X-ray crystallographic analysis. In both cases, the carboxylate anion X coordinates to the osmium centre to generate a distorted trigonal bipyramidal osmium(VIII) complex. The carboxylate adducts show a negative shift of the redox potentials ($E_{1/2}$) and a red shift of $v_{Os=O}$ stretches as compared to those of tetrahedral OsO₄ itself. Despite of the negative shift of $E_{1/2}$, the reactivity of these adduct complexes **1ˣ** was enhanced compared to OsO₄ in the benzylic C(sp³)–H bond oxidation. The reaction obeyed first-order kinetics both on **1ˣ** and the substrates, giving the second-order rate constants ($k_2$), which exhibit a linear correlation with the C–H bond dissociation energy ($BDE_{C–H}$) of the substrates (xanthene, 9,10-dihydroanthracene, fluorene and 1,2,3,4-tetrahydronaphthalene) and a kinetic deuterium isotope effect (KIE) of 9.2 ($k_2$(xanthene-$h_2$)/$k_2$(xanthene-$d_2$)). On the basis of these kientc data together with the DFT calculation results, we propose a *stepwise* reaction mechanism involving rate-limiting benzylic hydrogen atom abstraction and subsequent rebound of the generated organic radical intermediate to a remained oxido group on the osmium centre.

## Introduction

Activation of C(sp³)–H bonds is of great importance in synthetic organic chemistry, industrial chemistry and biological chemistry. Metal-oxido complexes with a high-oxidation state have been frequently employed as an oxidant in the oxidation of a variety of organic compounds in those systems. Osmium tetroxide (OsO₄) having the high oxidation state of VIII at the metal centre is a versatile oxidant in synthetic organic chemistry.[1-3] Majority of the oxidation reactions induced by OsO₄ is, however, *cis*-dihydroxylation and *cis*-aminohydroxylation of alkenes.[4-12] In 2005, Mayer and co-workers reported that OsO₄ can also induce oxygenation reaction of simple alkanes under an aqueous alkaline condition (pH = 12.1, at 85 °C for 7 days), where alkane substrates having a tertiary C–H bond (R₃C–H) are oxidised to the corresponding alcohols (R₃C–OH) whereas cyclic alkanes having secondary C–H bonds (R₂CH₂) such as cyclohexane and cyclopentane are converted to the ring-opened dicarboxylic acid derivatives.[13] They also reported oxidation of methane to methanol using an OsO₄/NaIO₄ system in water.[14] Although mechanistic details of such alkane oxygenation reactions have yet to be clarified, a hydroxide adduct of OsO₄, $[OsO_4(OH)]^-$, was proposed as an active oxidant in the alkane oxygenation reaction, where the C–H bond oxidation proceeds via a concerted [3 + 2] mechanism illustrated in Scheme 1(a). On the other hand, Lau and co-workers reported that an oxido-osmium(V) complex, $[Os^V(O)(qpy)(pic)Cl]^{2+}$ (qpy = 2,2':6',2'':6'',2'''-quaterpyridine; pic = 4-picoline), exhibited C(sp³)–H bond hydroxylation reactivity, for which they proposed hydrogen atom abstraction and subsequent OH rebound mechanism (Scheme 1(b)).[15]

Meanwhile, it has been demonstrated that the oxidation ability of OsO₄ in the *cis*-dihydroxylation is largely enhanced when Lewis base such as pyridine coordinates to the Os-metal centre.[16] We have also found that coordination of fluoride anion (F⁻) to OsO₄ enhances the reactivity toward alcohol oxidation reaction.[17] Thus, it is highly desired to explore the effects of external ligands in more detail in the alkane oxidation reaction by OsO₄.

In this study, we investigated the reactivity of carboxylate-adducts of OsO₄, $[OsO_4(X)]^-$ (**1ˣ**, acetate: X = AcO⁻ and benzoate: X = BzO⁻) in C(sp³)–H hydroxylation. Adoption of the carboxylate anion as the external ligand allowed us to perform isolation and structural characterisation of the anion adducts of OsO₄ as well as kinetic studies on the hydroxylation reactions of a series of alkane substrates. Combined with DFT calculations, we propose a mechanism involving two oxido groups, acting as the hydrogen atom acceptor from the alkane substrate (R–H) and the oxygen atom donor to the generated alkyl radical intermediate (R•), a stepwise version of the [3 + 2] mechanism.

## Experimental

**General.**

[a.] Department of Molecular Chemistry, Division of Applied Chemistry, Graduate School of Engineering, Osaka University, 2-1 Yamadaoka, Suita, Osaka 565-0871, Japan. E-mail: sugimoto@chem.eng.osaka-u.ac.jp, shinobu@chem.eng.osaka-u.ac.jp
[b.] Institute for Material Chemistry and Engineering and International Research Center for Molecular System, Kyushu University, 744 Motooka, Nishi-ku, Fukuoka, 819-0395, Japan. E-mail: kazunari@ms.ifoc.kyushu-u.ac.jp
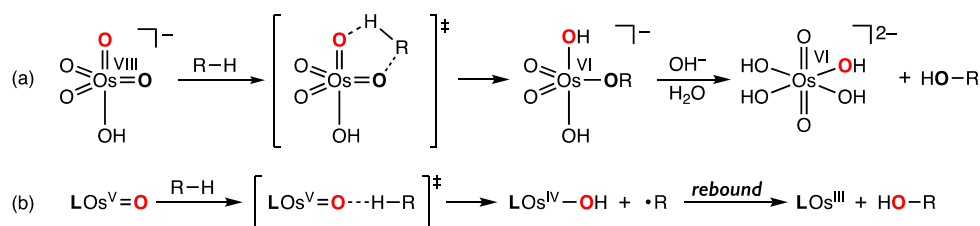
**Scheme 1.** Proposed mechanisms for C(sp$^3$)–H bond hydroxylation by osmium-oxido complexes.

The reagents and the solvents used in this study were commercial products of the highest available purity and further purified by the standard methods, if necessary.[18] $^1$H NMR spectra were recorded on a JEOL ECP400 or a JEOL ECS400 spectrometer. FT–IR spectra were recorded with a Jasco FT/IR–4100 spectrometer. Elemental analysis was carried out with a Yanaco CHN–Corder MT-5. UV-vis spectra were recorded on a Hewlett Packard 8453 photo diode array spectrometer or a Jasco V–650 spectrometer. Electrochemical measurements were performed with a Hokuto Denko HZ–7000. A set of carbon working electrode, an Ag/Ag$^+$ reference electrode, and a platinum counter electrode was employed in these experiments. After the CV measurements, ferrocene was added to the sample solution as an internal standard and the redox potential of Fc/Fc$^+$ was set as 0.0 V. A 0.1 M acetonitrile stock solution of OsO$_4$ was prepared by dissolving 1.0 g of OsO$_4$ (3.93 mmol) in 39.3 mL of acetonitrile and stored in a bottle with a screw cap. Products formed after the oxidation of substrates with osmium compounds were analysed with a HPLC system of an EXTREMA series (JASCO Co.) equipped with a reverse-phase column (column: Nacalai Co. COSMOSIL 5C$_{18}$-AR-II, eluent: CH$_3$CN / H$_2$O = 4 / 6). Ph$_4$POBz, [Ph$_4$P][Os$^{VII}$O$_4$] and deuterated xanthene (xanthene-$d_2$) were synthesized by reported methods.[19-22]

**Synthesis.**

**[Bu$_4$N][OsO$_4$(OAc)] (1$^{OAc}$).** Bu$_4$NOAc (60.3 mg, 0.20 mmol) was dissolved in a 2.0 mL of an acetonitrile stock solution containing 0.1 M OsO$_4$ (0.20 mmol), and the resultant solution was stirred for 15 min, during which colour of the solution became orange. Diethyl ether was added to the resultant orange solution to give an orange powder, which was collected by filtration and dried under air. Yield: 87.7 mg (0.16 mmol, 79%). Single crystals suitable for X-ray crystallographic analysis were obtained by slow diffusion of diethyl ether into a dichloromethane solution containing the product complex. Elemental analysis data did not match well with the calculated values because the orange powder changed to a black powder under air within a few hours. UV-vis (in-situ generated 1$^{OAc}$ in CH$_3$CN): $\lambda_{max}$ = 320 nm ($\varepsilon$ = 2560 M$^{-1}$ cm$^{-1}$), 390 (840 M$^{-1}$ cm$^{-1}$). FT–IR (KBr): 886 ($\nu_{(Os=O)asym}$) and 909 cm$^{-1}$ ($\nu_{(Os=O)sym}$). IR spectrum was measured quickly before the colour changed to black.

**[Ph$_4$P][OsO$_4$(OBz)] (1$^{OBz}$).** This compound was prepared according to a similar procedure described for synthesis of 1$^{OAc}$ by using Ph$_4$POBz (50.2 mg, 0.20 mmol) instead of Bu$_4$NOAc. The generated violet powder was collected by filtration and dried under air. Yield: 62.6 mg (0.12 mmol, 62%). Single crystals suitable for X-ray crystallographic analysis were obtained by

slow diffusion of diethyl ether into a dichloromethane solution containing the complex. Calcd.(C$_{31}$H$_{25}$O$_6$OsP):C, 52.09; H, 3.53 %. Found: C, 52.45, H, 3.58 %. UV-vis (CH$_3$CN): $\lambda_{max}$ = 320 nm ($\varepsilon$ = 2600 M$^{-1}$ cm$^{-1}$), 390 nm (800 M$^{-1}$ cm$^{-1}$). FT–IR (KBr): 886 ($\nu_{(Os=O)asym}$) and 906 cm$^{-1}$ ($\nu_{(Os=O)sym}$).

**Determination of formation constant ($K_f$) for Os-carboxylate adduct complexes 1$^X$.**

The titration of OsO$_4$ by Bu$_4$N$^+$X$^-$ (X = AcO$^-$ or BzO$^-$) was carried out in acetonitrile at 30 °C using a 1.0 cm path length UV-vis cell closed with a septum cap. Concentrations of the reagents are described in the figure captions of Figures 1 and S1. The formation constants of complexes 1$^{OAc}$ and 1$^{OBz}$ were calculated from the plots of $(A–A_0)/(A_\infty–A)$ against $[L]_0–\alpha[M]_0$ ($\alpha = (A–A_0)/(A_\infty–A_0)$), which is ordinary used to determine larger equilibrium constants,[23, 24] where $[M]_0$ is the initial concentration of OsO$_4$, $[L]_0$ is concentration of the Bu$_4$NX added, $A_0$ and $A_\infty$ are the initial and final absorbance, respectively, and $A$ is the observed absorbance at added [Bu$_4$NX] (eq. 1).

$$K_f([Bu_4NX]_0 - \alpha[OsO_4]_0) = \frac{A - A_0}{A_\infty - A} \qquad \left[ \alpha = \frac{A - A_0}{A_\infty - A_0} \right] \quad -(1)$$

**Kinetic studies.**

All reactions of 1$^{OAc}$ (0.5 mM) with the substrates (5.0–450 mM) were carried out in a 1.0 cm path length UV-cell closed with a septum cap. After generation of 1$^{OAc}$ by the treatment of OsO$_4$ (0.5 mM) with Bu$_4$NOAc (5.0 mM) in acetonitrile, reactions were started by adding the substrate into the solution through a septum cap with using a microsyringe at 70 °C under N$_2$ atmosphere. The reactions were followed by monitoring the increase of an absorption band around 694 nm due to an Os$^{VII}$ species. After the reaction, anisole was added into the resulting solution as an internal standard to analyse the products by HPLC. The yields of products were calculated by comparing the peak area of the products to those of the authentic samples using calibration curves.

**X-ray crystallographic analysis.**

The single crystal was mounted on a loop with a mineral oil, and all X-ray data were collected at –170 °C on a Rigaku R-AXIS RAPID diffractometer using filtered Mo-K$\alpha$ radiation. The structures were solved by direct method (SIR 2011) and expanded using Fourier techniques. The non-hydrogen atoms were refined anisotropically by full-matrix least-squares on $F^2$. The hydrogen atoms were attached at idealised positions on carbon atoms and were not refined. All of the crystallographic calculations were performed using the Crystal Structure software package of Molecular Structure Corp. [Crystal Structure, Crystal

Structure Analysis Package, version 3.8.1, Molecular Structure Corp. and Rigaku Corp. (2005)].

### Computational Details.

The density-functional-theory (DFT) calculations were performed with the Gaussian 16 program package (Rev. C01).[25] All geometry optimizations were carried out with the M06 functional.[26] We employed the SDD (Stuttgart/Dresden pseudopotentials) basis set[27, 28] for Os and the 6-311+G** basis set[29] for the other atoms. After geometry optimisations, vibrational analyses were calculated for all reaction species to confirm stable and transition structures. Energy profiles of calculated pathway are presented as the SCF energy considering the solvent effect of acetonitrile ($\varepsilon = 35.688$) based on the Polarizable Continuum Model (PCM).[30]

## Results and discussion

### Adduct formation of OsO$_4$ with carboxylate ions.

The reactions of OsO$_4$ with carboxylate ions, AcO$^-$ and BzO$^-$, were first examined. In Fig. 1(a) is shown the UV-vis spectral changes observed upon addition of various amounts of Bu$_4$NOAc to an acetonitrile solution of OsO$_4$ (0.5 mM) at 30 °C. OsO$_4$ has no absorption band in the visible region in CH$_3$CN, whereas an intense absorption band at 310 nm and a shoulder band at 390 nm gradually appeared as the amount of AcO$^-$ increased. The spectral change almost completed when total concentration of Bu$_4$NOAc reached about 4.0 mM, and the plot of $\Delta Abs$ against the concentration of Bu$_4$NOAc gave a saturation curve (Figure 1(a), inset), which can be analysed by using equation (1) (see Experimental section). Thus, the plot of $(A–A_0)/(A_\infty–A)$ against $[Bu_4NOAc]_0 – \alpha[OsO_4]_0$ gave a straight line as shown in Fig. 1(b), from which the formation constant $K_f^{OAc}$ of $1^{OAc}$ was calculated as $5.7 \times 10^3$ M$^{-1}$. The formation constant $K_f^{OBz}$ for $1^{OBz}$ was also determined as $5.4 \times 10^3$ M$^{-1}$ by a similar manner (Fig. S1). In both cases, the $K_f^X$ values are nearly the same, reflecting the similar p$K_a$ value of the conjugated acid (22.3 of AcOH and 20.7 of BzOH in CH$_3$CN).

### Crystal structures and spectroscopic characteristics of [OsO$_4$(X)]$^-$

The Os$^{VIII}$-carboxylate adducts, [Bu$_4$N][OsO$_4$(OAc)] ($1^{OAc}$) and [Ph$_4$P][OsO$_4$(OBz)] ($1^{OBz}$), were obtained as powder samples from the preparative scale reactions in acetonitrile (see Experimental section). The isolated carboxylate-adducts exhibited two strong IR bands ascribable to asymmetric ($\nu_{(Os=O)asym}$) and symmetric ($\nu_{(Os=O)sym}$) Os=O stretches at 886 and 909 cm$^{-1}$ for $1^{OAc}$ and 886 and 906 cm$^{-1}$ for $1^{OBz}$, respectively, in the solid state (KBr) (Fig. S2). These values are lower than those of OsO$_4$ itself (954 and 965 cm$^{-1}$),[31] reflecting weakened Os=O bonds due to electron donation by the carboxylate anion and/or decrement of the coordination number from 4 to 5. Furthermore, the $\nu_{Os=O}$ values of $1^{OAc}$ and $1^{OBz}$ are nearly the same due to similar degree of Os–X bonding interaction as reflecting in the Os–X bond lengths in the crystal structures as described below.

The crystal structures of $1^{OAc}$ and $1^{OBz}$ are shown in Fig. 2. The osmium centres are coordinated by the five oxygen atoms,
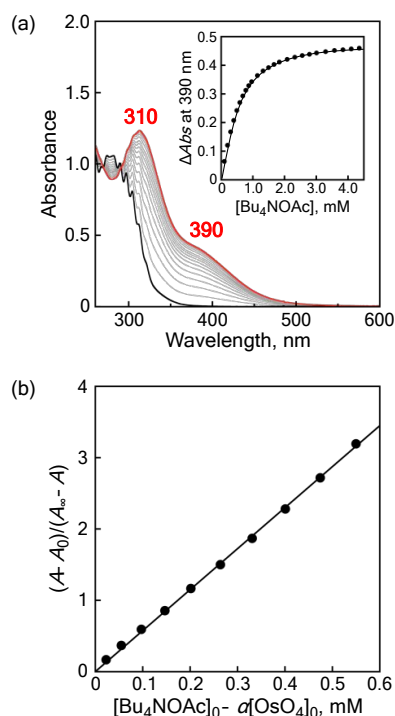


**Fig. 1** (a) UV-vis spectral changes observed in the titration of OsO$_4$ (0.5 mM) by Bu$_4$NOAc in acetonitrile at 30 °C. Inset: Plot of $\Delta Abs$ at 390 nm against [Bu$_4$NOAc]. (b) Plot of $(A–A_0)/(A_\infty–A)$ against $[Bu_4NOAc]_0 - \alpha[OsO_4]_0$.
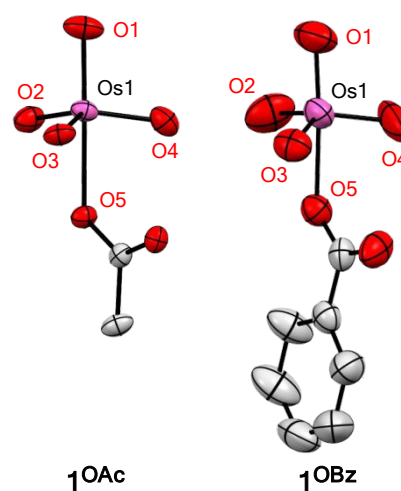


**Fig. 2** ORTEP drawings of $1^{OAc}$ and $1^{OBz}$ showing 50% probability thermal-ellipsoids. Hydrogen atoms and counter cation are omitted for clarity. Selected bond distances (Å) and angles (°): For $1^{OAc}$, Os(1)–O(1), 1.730(4); Os(1)–O(2), 1.709(3); Os(1)–O(3), 1.706(3); Os(1)–O(4), 1.707(3); Os(1)–O(5), 2.218(3); O(1)–plane(O2O3O4), 0.299; O(1)–Os(1)–O(5), 177.45(1); O(1)–Os(1)–O(2), 100.43(2); O(2)–Os(1)–O(3), 116.57(1); O(3)–Os(1)–O(4), 118.50(2). For $1^{OBz}$, Os(1)–O(1), 1.719(5); Os(1)–O(2), 1.691(4); Os(1)–O(3), 1.704(4); Os(1)–O(4), 1.701(5); Os(1)–O(5), 2.225(3); O(1)–plane(O2O3O4), 0.302; O(1)–Os(1)–O(5), 175.54(2); O(1)–Os(1)–O(2), 99.80(3); O(2)–Os(1)–O(3), 116.28(2); O(3)–Os(1)–O(4), 117.39(2).

four oxide oxygen atoms (O(1) to O(4)) and one carboxylate oxygen atom O(5). In $1^{OAc}$, the O(1)−Os(1)−O(5) angle is 177.45(1)°, and three bond angles of O(2)–Os(1)–O(3), O(2)–Os(1)–Os(4) and O(3)–Os(1)–O(4) are close each other (116.57(1), 115.93(2) and 118.50(2)°, respectively). The sum of the three bond angles is 351.0° and the Os(1) atom is located above the plane consisting of O(2), O(3) and O(4) atoms by 0.299 Å. The bond angles of O(1)–Os(1)–O(2), O(1)–Os(1)–O(3) and O(1)–Os(1)–O(4) also are very close each other (100.43(2), 100.28(2) and 99.56(2)°, respectively). It should be also noted that the Os(1)–O(1) bond is elongated upon coordination of AcO− anion to the Os(1) centre from 1.712 Å to 1.730(4) Å.[32] These observations reveal that the Os(1) centre adopts a slightly distorted trigonal-bipyramidal geometry having a O(1)–Os(1)–O(5) $C_{3v}$ axis. The overall structures of $1^{OBz}$ are similar to that of $1^{OAc}$ as shown in Fig. 2. In this case as well, the coordination of BzO− makes the osmium centre to adapt a slightly distorted trigonal bipyramidal structure.

**Electrochemical properties.**

The cyclic voltammetric (CV) measurements were performed to examine the electronic effects of coordinated carboxylate anions. OsO4 itself exhibited a reversible redox couple assignable to the Os(VIII)/Os(VII) redox process at $E_{1/2} = -0.32$ V (vs. Fc/Fc+, $E_{pa} = -0.28$ V, $E_{pc} = -0.35$ V, black line trace in Fig. 3). Addition of an excess amount of Bu4NOAc (10 mM) to the OsO4 (1.0 mM) solution gave a quasi-reversible redox wave in the negative region (red line trace), from which the redox potential of complex $1^{OAc}$ ($E_{1/2}$) was determined as –0.42 V (vs. Fc/Fc+, $E_{pa} = -0.37$ V, $E_{pc} = -0.46$ V). $1^{OBz}$ also gave a quasi-reversible redox couple (Fig. S3), from which $E_{1/2}$ values was determined as –0.42 V (vs. Fc/Fc+, $E_{pa} = -0.38$ V, $E_{pc} = -0.46$ V). The redox potential shifted to the negative direction compared to that of OsO4, indicating that the coordination of the carboxylate anion makes the osmium centre harder to be reduced. Such a negative shift of the redox potential ($\Delta E = 0.10$ V) demonstrates that the electron-transfer oxidation power of complex $1^{OAc}$ and $1^{OBz}$ decreases by 9.6 kJ mol−1.

**Oxidation of C(sp³)–H bonds by $1^X$**

The oxidation ability of $1^{OAc}$ and $1^{OBz}$ was examined in the oxidation of xanthene. In Fig. 4(a) is shown the UV-vis spectral changes observed in the reaction of OsO4 (0.5 mM) and xanthene
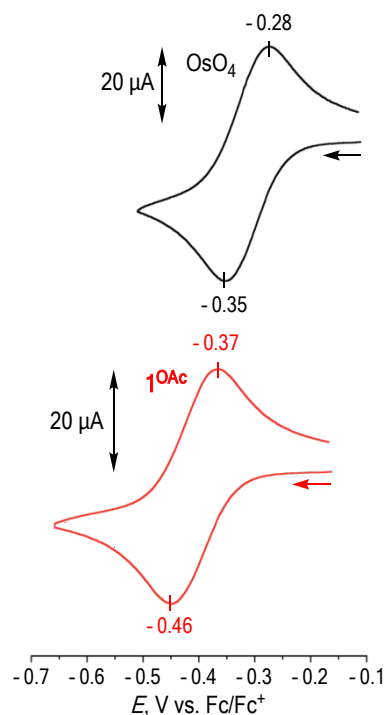


**Fig. 3** Cyclic voltammograms of OsO4 (1.0 mM, black line trace) and that in the presence of Bu4NOAc (10 mM, red line trace) in CH3CN containing 0.1 M of Bu4NPF6 as the electrolyte at a scan rate of 100 mV/sec 25 °C.

(15 mM) in the presence of Bu4NOAc (20 mM) in CH3CN at 70 °C under N2 atmosphere. Under this reaction condition, almost all OsO4 is converted to the acetate adduct $1^{OAc}$ based on the $K_f^{OAc}$ value determined by the titration at 70 °C (Fig. S4, $K_f^{OAc}$ = 1.3 × 10³ M−1 at 70 °C in CH3CN). The shoulder band around 390 nm due to $1^{OAc}$ decreased with concomitant increase of a new absorption bands at 573, 660 and 694 nm. These bands are similar to those of the authentic sample of [OsVIIO4]− (Fig. S5), the formation of which was confirmed by ESI–MS of the resultant solution (Fig. S6). [OsVIIO4]− can be generated by the comproportionation reaction between OsVI species and remained $1^{OAc}$ as discussed below.[33] From the final reaction solution, xanthone (ketone) and xanthydrol (alcohol) were obtained in a 13 and a 22% yield based on OsO4, respectively (Table 1). Since xanthone and xanthydrol are four-electron and two-electron
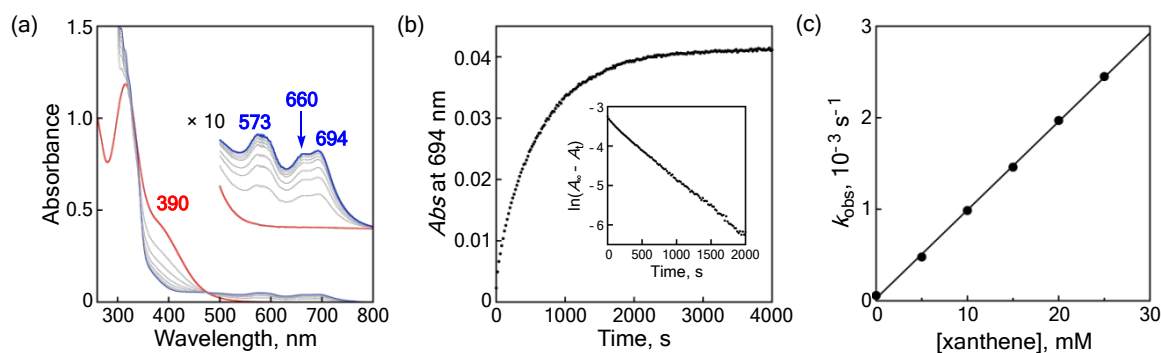


**Fig. 4** (a) UV–vis spectral change of $1^{OAc}$ ([OsO4]0 = 0.5 mM, [Bu4NOAc]0 = 20 mM) observed upon addition of xanthene (15 mM) in CH3CN at 70 °C under N2 atmosphere. (b) The time course of the growth of OsVII species monitored at 694 nm ([xanthene] = 15 mM). Inset: Plot of ln($A_\infty - A_t$) against the reaction time. (c) Plot of $k_{obs}$ against [xanthene].
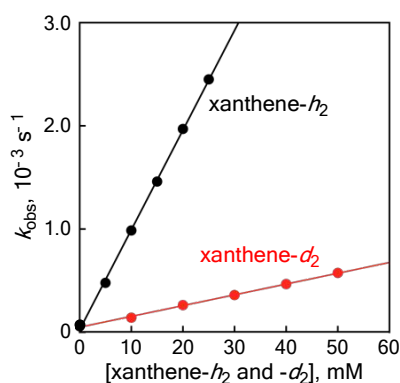
**Fig. 5** Plots of $k_{obs}$ against [xanthene-$h_2$] and [xanthene-$d_2$].

oxidation products, respectively, the product yields based on the oxidation equivalent are 52 and 44%, respectively (total 96%). A similar result was obtained in the oxidation of xanthene by $1^{OBz}$ (Table S1). On the other hand, such oxidation products were hardly obtained in the reaction of OsO$_4$ itself and xanthene
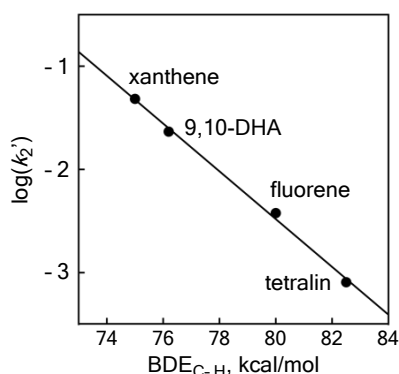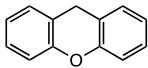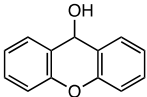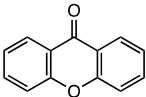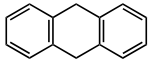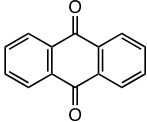


**Fig. 6** Plot of $\log(k_2')$ against BDE$_{C-H}$ for the oxidation of a series of substrates.

under the same reaction condition (Table S1). Thus, it is apparent that the adduct formation greatly enhances the reactivity of OsO$_4$ in the C(sp$^3$)–H bond oxidation reaction. Such an enhancement of oxidation ability of OsO$_4$ was also observed in alkene *cis*-dihydroxylation 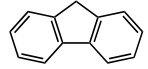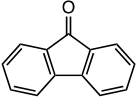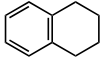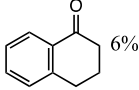when pyridine was added to the reaction solution.[16] These phenomena are notable because the adduct formation causes the decrease of the electron-transfer oxidation ability of OsO$_4$ as mentioned above (Fig. 3 and Fig. S3). Thus, the oxidation of xanthene by $1^{OAc}$ and $1^{OBz}$ was further investigated kinetically to get further insights into the reaction mechanism.

The time course of the absorption changes at 694 nm is shown in Fig. 4(b). The pseudo-first order rate constants ($k_{obs}$) were then determined by the plots of $\ln(\Delta A)$ against the reaction time as shown in Fig. 4(b) (inset). Then, the plot of $k_{obs}$ against the concentrations of xanthene gave a straight line (Fig. 4(c)), from the slope of which the second-order rate constant ($k_2$) was determined as $9.7 \times 10^{-2}$ M$^{-1}$ s$^{-1}$. The reaction of $1^{OBz}$ with xanthene were analysed in the same way to get $k_2 = 7.6 \times 10^{-2}$ M$^{-1}$ s$^{-1}$ at 70 °C, where $K_f^{OBz}$ at 70 °C was also determined as $1.0 \times 10^3$ M$^{-1}$ by a similar manner in the case of $1^{OAc}$ (Fig. S7 and S8). Since $1^{OAc}$ and $1^{OBz}$ showed similar reactivity, further kinetic studies were performed using $1^{OAc}$.

The second-order rate constant $k_2^D$ was determined as $1.0 \times 10^{-2}$ M$^{-1}$ s$^{-1}$ using xanthene-$d_2$ (Fig. 5 and Fig. S9). Thus, the kinetic deuterium isotope effect (KIE = $k_2^H/k_2^D$) was determined as 9.7, indicating that the C(sp$^3$)–H bond cleavage of xanthene is involved in the rate determining step. In addition to xanthene (BDE$_{C-H}$ = 75.0 kcal mol$^{-1}$), oxidation of 9,10-dihydroanthracene (BDE$_{C-H}$ = 76.2 kcal mol$^{-1}$), fluorene (BDE$_{C-H}$ = 80.0 kcal mol$^{-1}$) and 1,2,3,4-tetrahydronaphthalene (tetralin) (BDE$_{C-H}$ = 82.5 kcal mol$^{-1}$) were also investigated in the same manner (Fig. S10–12), and the normalised second-order rate constant ($k_2'$) of each substrate was obtained by dividing the

**Table 1.** Rate constants and products of the oxidation of C(sp$^3$)–H substrates by $1^{OAc}$.

| Substrate[a] | BDE$_{C-H}$ (kcal/mol) | $k_2$ (M$^{-1}$ s$^{-1}$) | $k_2'$ (M$^{-1}$ s$^{-1}$) | Product[b] and Yield[c] |
|---|---|---|---|---|
|  | 75.0 | $9.7 \times 10^{-2}$ | $4.8 \times 10^{-2}$ |  22% (44%)   13% (52%) |
|  | 76.2 | $9.3 \times 10^{-2}$ | $2.3 \times 10^{-2}$ |  12% (96%) |
|  | 80.0 | $7.6 \times 10^{-3}$ | $3.8 \times 10^{-3}$ |  19% (76%) |
|  | 82.5 | $3.2 \times 10^{-3}$ | $0.81 \times 10^{-3}$ |  6% (24%) |

[a] Reaction conditions: [$1^{OAc}$] = 0.5 mM (1.0 μmol / 2.0 mL) in the oxidation of xanthene (5.0 mM), [$1^{OAc}$] = 1.0 mM (2.0 μmol / 2.0 mL) in the oxidation of 9,10-dihydroanthracene (10 mM), fluorene (50 mM) and tetralin (200 mM) in CH$_3$CN at 70 °C for 2 h under N$_2$. [b] Products were detected by HPLC or $^1$H NMR. [c] Numbers shown in the parenthesis are the yields based on the oxidation equivalent.
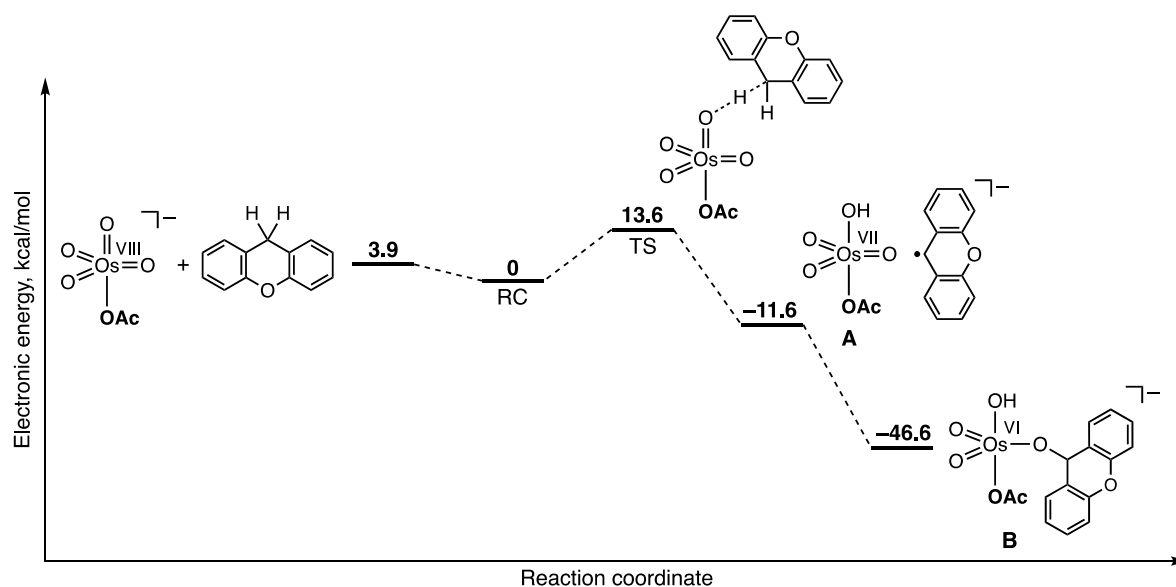
**Fig. 7** Computed energy diagrams for the oxidation of xanthene by $1^{OAc}$ in the singlet state.

observed second-order rate constant $k_2$ with the number of equivalent C(sp$^3$)–H bond in the substrate (Fig. S13). Fig. 6 shows the plot of log($k_2$') against the BDE$_{C–H}$ of the substrates. As clearly seen, there is a good linear corelation between them, strongly supporting that the reaction involves the C–H bond cleavage in the rate-limiting process.

Notably, the keto-products were obtained as the major products in the oxidation of 9,10-dihydroanthracene, fluorene and tetralin by $1^{OAc}$ (Table 1). For instance, anthraquinone was obtained in a 12% yield based on OsO$_4$, which corresponds to a 96% yield based on the oxidation equivalent, since anthraquinone is 8-electron oxidation product (12% × 8 = 96%). The yields of fluorene and $\alpha$-tetralone (four-electron oxidation products) are 76 and 24% based on the oxidation equivalent, respectively. In the oxidation of tetralin, some oxidation products besides $\alpha$-tetralone were observed by HPLC, however, they could not be identified.

To get insights into the oxidation mechanism, density functional theoretical (DFT) calculations were performed. Except for **A** + radical species, which is the open-shell singlet state, the ground state is the closed-shell singlet state. The calculated energy diagram and optimized structures in each step are shown in Fig. 7 and S14, respectively. First, a reactant complex (RC) was generated between $1^{OAc}$ and xanthene. Then, hydrogen atom abstraction takes place by the oxido group at the axial position of $1^{OAc}$ *via* a transition-state (TS) with an activation barrier of 13.6 kcal/mol to produce hydroxido-osmium(VII) species **A** and a radical intermediate of the substrate. In the final step, the radical carbon atom binds to one of the three equatorial oxido groups of **A** with nearly barrierless in energy to form alkoxide product **B** (Fig. S15). The formation of **B** from RC is an exothermic reaction of 46.6 kcal/mol. These computed results indicated that the oxygen atom of the alcohol product is derived from one of the oxido groups in $1^{OAc}$.

In general, oxidation of 9,10-dihydroanthracene with metal-oxido complexes gives anthracene as the major product, which is formed by hydrogen atom abstraction and subsequent rapid

aromatisation.[34-38] On the other hand, the reaction of 9,10-dihydroanthracene and $1^{OAc}$ only gave the oxygenated product, 9,10-anthraquinone (Table 1). Other substrates also gave the oxygenated products (Table 1). Thus, the bond formation between one oxido group of **A** and the carbon radical intermediate, generated by the initial hydrogen atom abstraction, may be much faster than the aromatisation process. Then, alcohol product was dissociated from the alkoxide adduct **B** to give Os$^{VI}$ species such as [Os$^{VI}$(O)$_3$(OAc)]$^-$. The generated Os$^{VI}$ species may be oxidised by remained [Os$^{VIII}$O$_4$(OAc)]$^-$ to give [Os$^{VII}$O$_4$]$^-$, Os$^{VII}$(O)$_3$(OAc) and AcO$^-$ as experimentally detected as the final products (Fig. 4(a) and Scheme S1). On the other hand, the alcohol products may be immediately oxidized by $1^X$ to give the keto-products.

## Summary

In the present study, the reactions of OsO$_4$ with carboxylate anions (AcO$^-$ and BzO$^-$) were examined to investigate the anion coordination effects on the structure, physicochemical properties and oxidation reactivity. The carboxylate anions formed stable 1 : 1 adducts with OsO$_4$, $1^X$ with the formation constants of $K_f^{OAc}$ = 5.7 × 10$^3$ M$^{-1}$ and $K_f^{OBz}$ = 5.4 × 10$^3$ M$^{-1}$. Structures of the 1 : 1 adduct $1^X$ were determined by X-ray crystallographic analysis as a slightly distorted trigonal bipyramid structure. The strong interaction induces the negative shift of the redox potentials of $1^{OAc}$ and $1^{OBz}$ in the cyclic voltammetric measurements. Nonetheless, these adducts showed a higher reactivity in the oxidation of benzylic oxidation of C(sp$^3$)–H bonds compared to OsO$_4$ itself. Kinetics and DFT calculation studies indicated that the reaction proceeds *via* hydrogen atom abstraction from the benzylic position of the substrate by the axial oxido group of $1^{OAc}$ and subsequent bond formation between carbon-centre radical and one of the equatorial oxido ligands of Os$^{VII}$–hydroxido species **A** to give alkoxido-adduct **B** (Fig. 7). The enhancement of the C(sp$^3$)–H oxidation ability of OsO$_4$ can be

attributed to the increase of reactivity of the axial oxido group by strong anion coordination from *trans*-position, as reflected with the elongation of Os(1)–O(1) bond length (1.70 Å → 1.73 Å) and red shifts of $v_{Os=O}$ stretches by carboxylate anion coordination to $OsO_4$. These effects may enhance the hydrogen atom abstraction. The subsequent radical rebound to one of the oxido group at the equatorial position may also be enhanced by the structural distortion from tetrahedron to trigonal bipyramid. Namely, the steric relation between the oxygen atom of the oxido group and the carbon centre radical in intermediate **A** may be favourable to induce the oxygen rebound process and prevent the aromatisation reaction. The present studies give deeper insights into the [3 + 2] type alkane hydroxylation mechanism by with the anion-adducts of $OsO_4$.

## Conflicts of interest

There are no conflicts to declare.

## Acknowledgements

## References

1. H. C. Kolb, M. S. VanNieuwenhze and K. B. Sharpless, *Chem. Rev.*, 1994, **94**, 2483-2547.
2. H. C. Kolb and K. B. Sharpless, *Transition Metals for Organic Synthesis*, 2004, 309-336.
3. B. S. Pilgrim and T. J. Donohoe, *J. Org. Chem.*, 2013, **78**, 2149-2167.
4. N. A. Milas and S. Sussman, *J. Am. Chem. Soc.*, 1936, **58**, 1302-1304.
5. K. B. Sharpless, D. W. Patrick, L. K. Truesdale and S. A. Biller, *J. Am. Chem. Soc.*, 1975, **97**, 2305-2307.
6. K. B. Sharpless and K. Akashi, *J. Am. Chem. Soc.*, 1976, **98**, 1986-1987.
7. V. VanRheenen, R. C. Kelly and D. Y. Cha, *Tetrahedron Lett.*, 1976, **17**, 1973-1976.
8. K. B. Sharpless, A. O. Chong and K. Oshima, *J. Org. Chem.*, 1976, **41**, 177-179.
9. K. Akashi, R. E. Palermo and K. B. Sharpless, *J. Org. Chem.*, 1978, **43**, 2063-2066.
10. E. Herranz, S. A. Biller and K. B. Sharpless, *J. Am. Chem. Soc.*, 1978, **100**, 3596-3598.
11. R. Ray and D. S. Matteson, *Tetrahedron Lett.*, 1980, **21**, 449-450.
12. S. G. Hentges and K. B. Sharpless, *J. Org. Chem.*, 1980, **45**, 2257-2259.
13. B. C. Bales, P. Brown, A. Dehestani and J. M. Mayer, *J. Am. Chem. Soc.*, 2005, **127**, 2832-2833.
14. T. Osako, E. J. Watson, A. Dehestani, B. C. Bales and J. M. Mayer, *Angew. Chem., Int. Ed.*, 2006, **45**, 7433-7436.
15. Y. Liu, S.-M. Ng, W. W. Y. Lam, S.-M. Yiu and T.-C. Lau, *Angew. Chem., Int. Ed.*, 2016, **55**, 288-291.
16. D. W. Nelson, A. Gypser, P. T. Ho, H. C. Kolb, T. Kondo, H.-L. Kwong, D. V. McGrath, A. E. Rubin, P.-O. Norrby, K. P. Gable and K. B. Sharpless, *J. Am. Chem. Soc.*, 1997, **119**, 1840-1858.
17. T. Fujimoto, Y. Hirata, H. Sugimoto, M. Miyanishi, Y. Shiota, K. Yoshizawa and S. Itoh, *Bull. Chem. Soc. Jpn.*, *in press*, (doi:10.1246/bcsj.20210377).
18. N. Bernier, S. Carvalho, F. Li, R. Delgado and V. Félix, *J. Org. Chem.*, 2009, **74**, 4819-4827.
19. K. Harada, Y. Imbe, K. Nishihira, S. Tanaka, S. Fujitsu, R. Sugise, K. Kashiwagi, T. Sumida, T. Doi, M. Nishio, US Pat., 5,892,091, 1999.
20. E. Bilger, J. Pebler, R. Weber and K. Dehnicke, *Z. Naturforsch. Teil. B*, 1984, **39**, 259-261.
21. H. Gao and J. T. Groves, *J. Am. Chem. Soc.*, 2017, **139**, 3938-3941.
22. M. A. Ehudin, D. A. Quist and K. D. Karlin, *J. Am. Chem. Soc.*, 2019, **141**, 12558-12569.
23. S. Itoh, H. Kawakami and S. Fukuzumi, *Biochemistry*, 1998, **37**, 6562-6571.
24. S. Itoh, M. Taniguchi and S. Fukuzumi, *Chem. Commun.*, 2000, 329-330.
25. M. J. Frisch, G. W. Trucks, H. B. Schlegel, G. E. Scuseria, M. A. Robb, J. R. Cheeseman, G. Scalmani, V. Barone, G. A. Petersson, H. Nakatsuji, X. Li, M. Caricato, A. V. Marenich, J. Bloino, B. G. Janesko, R. Gomperts, B. Mennucci, H. P. Hratchian, J. V. Ortiz, A. F. Izmaylov, J. L. Sonnenberg, Williams, F. Ding, F. Lipparini, F. Egidi, J. Goings, B. Peng, A. Petrone, T. Henderson, D. Ranasinghe, V. G. Zakrzewski, J. Gao, N. Rega, G. Zheng, W. Liang, M. Hada, M. Ehara, K. Toyota, R. Fukuda, J. Hasegawa, M. Ishida, T. Nakajima, Y. Honda, O. Kitao, H. Nakai, T. Vreven, K. Throssell, J. A. Montgomery Jr., J. E. Peralta, F. Ogliaro, M. J. Bearpark, J. J. Heyd, E. N. Brothers, K. N. Kudin, V. N. Staroverov, T. A. Keith, R. Kobayashi, J. Normand, K. Raghavachari, A. P. Rendell, J. C. Burant, S. S. Iyengar, J. Tomasi, M. Cossi, J. M. Millam, M. Klene, C. Adamo, R. Cammi, J. W. Ochterski, R. L. Martin, K. Morokuma, O. Farkas, J. B. Foresman and D. J. Fox, *Journal*, 2016.
26. Y. Zhao and D. G. Truhlar, *Theor. Chem. Acc.*, 2008, **120**, 215-241.
27. M. Dolg, U. Wedig, H. Stoll and H. Preuss, *J. Chem. Phys.*, 1987, **86**, 866-872.
28. D. Andrae, U. Häußermann, M. Dolg, H. Stoll and H. Preuß, *Theoret. Chim. Acta*, 1990, **77**, 123-141.
29. R. Krishnan, J. S. Binkley, R. Seeger and J. A. Pople, *J. Chem. Phys.*, 1980, **72**, 650-654.
30. M. Cossi, V. Barone, R. Cammi and J. Tomasi, *Chem. Phys. Lett.*, 1996, **255**, 327-335.
31. L. A. Woodward and H. L. Roberts, *Trans. Faraday Soc.*, 1956, **52**, 615-619.
32. H. M. Seip, *Selected Topics in Structure Chemistry*, ed. P. Anderson, O. Bastiansen and S. Furberg, Oslo: Universitetsforlaget, 1967, p. 25.
33. T. E. Geswindt, W. J. Gerber, H. E. Rohwer and K. R. Koch, *Dalton Trans.*, 2011, **40**, 8581-8588.
34. J. R. Bryant and J. M. Mayer, *J. Am. Chem. Soc.*, 2003, **125**, 10351-10361.
35. T. H. Parsell, M.-Y. Yang and A. S. Borovik, *J. Am. Chem. Soc.*, 2009, **131**, 2762-2763.
36. A. Company, I. Prat, J. R. Frisch, D. R. Mas-Ballesté, M. Güell, G. Juhász, X. Ribas, D. E. Münck, J. M. Luis, L. Que Jr and M. Costas, *Chem. Eur. J.*, 2011, **17**, 1622-1634.
37. S. Hong, F. F. Pfaff, E. Kwon, Y. Wang, M.-S. Seo, E. Bill, K. Ray and W. Nam, *Angew. Chem., Int. Ed.*, 2014, **53**, 10403-10407.
38. B. Wang, Y.-M. Lee, W.-Y. Tcho, S. Tussupbayev, S.-T. Kim, Y. Kim, M. S. Seo, K.-B. Cho, Y. Dede, B. C. Keegan, T. Ogura, S. H. Kim, T. Ohta, M.-H. Baik, K. Ray, J. Shearer and W. Nam, *Nat. Commun.*, 2017, **8**, 14839.